Journal of Materials Chemistry C

RSC Publishing

PAPER

View Article Online
View Journal

Cite this: DOI: 10.1039/c3tc31743a

Highly efficient deep-blue organic electroluminescent devices ($CIE_y \approx 0.08$) doped with fluorinated 9,9′-bianthracene derivatives (fluorophores)

Yue Yu,[a] Zhaoxin Wu,*[a] Zhanfeng Li,[ab] Bo Jiao,[a] Lu Li,[a] Lin Ma,[a] Dongdong Wang,[c] Guijiang Zhou*[c] and Xun Hou[a]

A series of new fluorinated 9,9′-bianthracene derivatives (BAnFs) have been designed and synthesized to serve as deep-blue dopants in organic electroluminescent (EL) devices. With the different substitution patterns of the electron-withdrawing groups, such as F and CF_3, the photophysical properties, the energy levels and thermal stability of these BAnFs are tuned, which are supported by a density functional study of their geometry and electronic structure. In the thin film state, the fluorescent emissions of the BAnFs are fine-tuned from 448 to 439 nm, with varied fluorinated phenyl rings attached to the 9,9′-bianthracene core. All the BAnFs show a considerable thermal stability, which have high T_g values, above 150 °C. A pure blue emission at the Commission Internationale de l'Éclairage (CIE) coordinates (0.156, 0.083), has been achieved using the host 4,4′-bis(*N*-carbazolyl)biphenyl (CBP) doped with 10,10′-bis(3,5-bis(trifluoromethyl)phenyl)-9,9′-bianthracene (BAn-(3,5)-CF_3). The maximum current efficiency and power efficiency of the BAn-(3,5)-CF_3-doped device are 3.05 cd A^{-1} and 2.62 lm W^{-1}, corresponding to 5.02% of the maximum external quantum efficiency. The synthesized new fluorinated 9,9′-bianthracene derivatives show potential applications as highly efficient pure blue emitters for organic light emitting devices.

Received 5th September 2013
Accepted 10th October 2013

DOI: 10.1039/c3tc31743a

www.rsc.org/MaterialsC

1. Introduction

Organic light-emitting diodes (OLEDs) have shown great potential as a technology of the next generation for flat-panel displays and solid-state lighting, since the first report by Tang and Van Slyke.[1–4] For a full-color display and white lighting, it is essential to have the three primary colors, red (R), green (G), and blue (B). However, progress in highly efficient blue OLEDs is far behind the counterparts of green/red OLEDs, due to the difficulty in developing blue-emitting materials with a high efficiency, color purity, and long operation time. Deep-blue emitters with a high quantum efficiency are needed to effectively reduce power consumption and to increase the color gamut of full-color OLEDs. A deep-blue emitter can also be utilized to generate light of other colors by an energy cascade to a suitably emissive dopant.[5] Therefore, the development of saturated deep-blue (CIE_y coordinate < 0.10) emitters with a high efficiency is highly crucial for realizing efficient OLEDs and has become an intensive studied subject at present.

It is well known that a dopant–host doped emitter system can significantly avoid the concentration quenching of fluorescence and improve the device performance in terms of the electroluminescent (EL) efficiency and emissive color, as well as the operational lifetime.[6] Various blue host materials and their non-doped EL devices have been reported to date, which include anthracene, fluorene, styrylarylene, pyrene, quinoline and triphenylene derivatives.[7–12] Among these, the anthracene-cored fluorescent emitters with an intrinsically wide-energy band gap, high fluorescence quantum yield, and high thermal stability as well as non-dispersive ambipolar carrier transporting properties, have attracted considerable interest as deep-blue OLEDs.[7] Although many kinds of blue host materials have been developed, with some of them providing highly efficient blue EL with CIE coordinates near the National Television System Committee (NTSC) standard blue coordinates (0.14, 0.08),[13] suitable dopants that emit light in the deep blue region are still rare. Only a little research has been reported on the utilization of anthracene derivatives as blue dopants in OLED applications.[14]

9,9′-Bianthracene, made up of two anthracene units linked by a single bond at the 9- and 9′-position, is an anthracene derivative. Crystallographic information reveals that the two anthracene rings are almost perpendicular to each other, with a

[a]Key Laboratory of Photonics Technology for Information, School of Electronic and Information Engineering, Xi'an Jiaotong University, Xi'an 710049, People's Republic of China. E-mail: zhaoxinwu@mail.xjtu.edu.cn; Fax: +86 029-82664867

[b]College of Physics and Optoelectronics, Taiyuan University of Technology, Taiyuan 030024, People's Republic of China

[c]Department of Chemistry, School of Science, Xi'an Jiaotong University, Xi'an 710049, People's Republic of China. E-mail: zhougj@mail.xjtu.edu.cn

dihedral angle of 89.4° due to the strongly repulsive interaction of the hydrogen atoms at the 1,1′- and 8,8′-positions.[15] Over the past four decades, many studies have focussed on its photophysical properties in solution.[16] The two anthracene groups are electronically decoupled because of the orthogonal structure in the ground state, while they exhibit a strong electronic interaction with the relaxation of the geometric structure in the excited state.[17] The 9,9′-bianthracene-cored fluorescence emitters with particular twisted intramolecular charge transfer (TICT) characteristics realize the electron–hole recombination *via* an intramolecular conversion from charge-transfer excitons (immediate precursor) to a radiative singlet exciton (final state).[18] Fluorination has been used in the past decade as a route to induce stability and electron transport or ambipolar transport in organics by lowering the energy levels in the small molecules or polymers, especially for OLEDs. It also has been used to adjust the emission spectrum and fluorescence quantum yields (Φ_f).[19–24] With different substitution patterns of electron-withdrawing groups, such as F and CF_3, the photophysical properties, the energy levels and thermal stability are tuned.[24]

In the paper, we reported the synthesis, characterization, and EL properties of new blue materials based on a 9,9′-bianthracene core and various fluorinated end-capping groups. These fluorinated 9,9′-bianthracene derivatives (BAnFs) exhibit satisfactory EL characteristics, and their emission wavelengths can be finely tuned in the deep-blue region. The BAn-(3,5)-CF_3-doped device attains an EQE of 5.02% with excellent CIE coordinates (0.156, 0.083), that meet the NTSC standard blue coordinates.

2. Results and discussion

2.1 Synthesis, structure characterization and theoretical computation

A series of new BAnFs were readily obtained with a one-step Suzuki coupling between brominated 9,9′-bianthracene (BAn-2Br) and the respective fluorinated phenylboronic in the presence of a palladium catalyst, with yields ranging from 83% to 96%. The chemical structures and the synthetic routes of the BAnFs in this study are shown in Scheme 1. We systematically synthesized six compounds by changing the number and position of the varied F or CF_3 substituents on the two phenyl rings attached at the 10,10′-positions of the 9,9′-bianthracene core. After purification by column chromatography and recrystallization, these newly synthesized BAnFs were purified further by train sublimation at a reduced pressure below 10^{-3} Pa and fully characterized with ^{1}H NMR spectroscopy and elemental analysis. High-pressure liquid chromatography (HPLC) analysis was carried out to check the purity of the materials, which was, at least, above 99.5%.

To understand the optimized geometry and electronic structures of the BAnFs, we carried out density functional theory (DFT) calculations at the B3LYP/6-31G(d,p) level in the Gaussian 09 program. As shown in Fig. 1, the electron densities of the HOMO and LUMO are mostly localized on the two anthracene units, implying that the absorption and emission processes are mainly attributed to the π–π* transition of the 9,9′-bianthracene moiety. Thus, the excellent luminescence efficiency of the 9,9′-bianthracene moiety can be maintained. The calculated HOMOs and LUMOs of all the BAnFs are listed in Table 1. In each BAnF, the two adjacent planar anthracene units are nearly perpendicular to each other because of a steric repulsion of the anthracene *peri*-hydrogen atoms (1,1′- and 8,8′-positions). For BAn-(2)-F and BAn-(2,4)-F, the dihedral angles between the functionalized phenyl rings and the adjacent phenyl rings of the 9,9′-bianthracene core, are 85° and 76°, respectively, which are slightly smaller than those of other BAnFs (90°). This discrepancy can be explained by the intramolecular F···H interactions of the F atoms in the *ortho*-positions of the peripheral substituted phenyl, with the H atoms of the anthracene unit in BAn-(2)-F and BAn-(2,4)-F. The calculation results indicate that the BAnFs have extremely twisted geometry configurations, which can prevent intramolecular extending of the π-electrons and suppress intermolecular interactions, conjugation, and molecular recrystallization.

2.2 Thermal properties

Their thermal properties were investigated by differential scanning calorimetry (DSC), and the resultant data, including melting temperature (T_m) and glass-transition temperature (T_g), are shown in Table 1. The T_gs of compounds BAn-(2)-F, BAn-(3)-F, BAn-(4)-F, and BAn-(2,4)-F were determined to be 168, 167, 167, and 156 °C, respectively, by DSC in the second heating scans (for THE details, see Fig. 2). BAn-(3,4,5)-F did not exhibit a glass transition up to the T_m, and in the DSC curves of BAn-(3,5)-CF_3, no T_g and T_m were observed, although the compound was heated to 420 °C. The T_ms of compounds BAn-(2)-F, BAn-(3)-F, BAn-(4)-F, BAn-(2,4)-F and BAn-(3,4,5)-F were determined to be 328, 362, 347, 322, and 387 °C, respectively. The high stability of the amorphous glass state of these compounds is attributed to the non-planarity of their molecular structures, demonstrating that the perpendicular-type 9,9′-bianthracene core improves the thermal stability efficiently. Therefore, thermal analyses indicate that these chromophores are thermally stable and suitable for vapor deposition in OLEDs fabrication.

2.3 Photophysical properties

Fig. 3 shows the normalized UV-vis absorption and photoluminescence (PL) spectra of the BAnFs in dichloromethane (CH_2Cl_2) dilute solutions and films (*ca.* 50 nm), obtained by thermal evaporation on a pre-cleaned quartz substrate. Their photophysical data are summarized in Table 1. All the compounds show very similar absorption peaks in CH_2Cl_2 dilute solutions. The UV-vis absorption spectra (Fig. 3a) in CH_2Cl_2 solutions show that all of the BAnFs exhibit the common isolated characteristic vibronic structure at approximately 400, 379, 358, 340 nm, due to the 9,9′-bianthracene core. Additionally, the absorption bands with the most prominent peak appearing at 260 nm are attributed to the substituted aryl groups. The absorption spectra of these F-substituted BAnFs (*i.e.*, BAn-(2)-F, BAn-(3)-F, BAn-(4)-F, BAn-(2,4)-F and BAn-(3,4,5)-F) in films are slightly red-shifted by 3–5 nm relative to those in

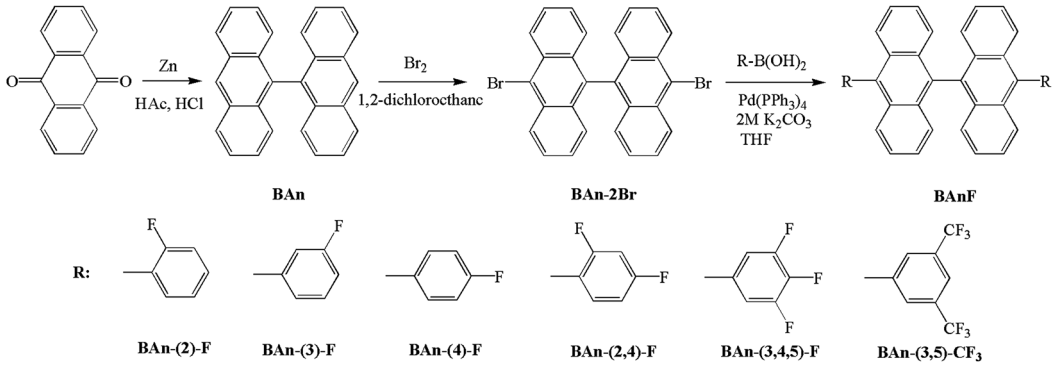

Scheme 1 Synthesis and structures of the BAnF compounds.

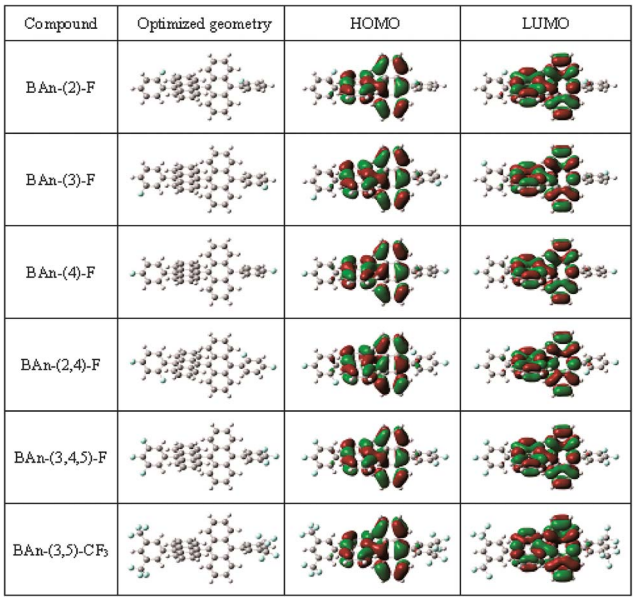

Fig. 1 The optimized geometries and the molecular orbital surfaces of the HOMOs and LUMOs for the BAnFs obtained at the B3LYP/6-31G level.

solutions. However, the absorption spectra of the BAn-(3,5)-CF_3 show no spectral red shift going from CH_2Cl_2 solution to the thin-film state. The similarity between the absorption spectra of the dilute solutions and thin films suggests that the conformation of the solid state of the BAnFs is similar to that of the solution state of the BAnFs, which is attributed to its non-coplanar structure, reducing the degree of intermolecular aggregation and π-delocalization.

The PL maximum in the CH_2Cl_2 dilute solutions varies depending on the number and position of the F or CF_3 substituents in the BAnFs. The PL spectra of the *meta*-position on the phenyl ring with respect to the fluorine atom in the mono-substituted molecule, BAn-(3)-F, appear to be blue-shifted with the most prominent peak appearing at 445 nm when compared with those of the *ortho*-position in BAn-(2)-F (λ_{max} = 449 nm), the *para*-position in BAn-(4)-F (λ_{max} = 449 nm), and the *ortho*- and *para*-positions in BAn-(2,4)-F (λ_{max} = 448 nm). This is attributed to the double nature of the electronic effect of the fluorine atom, which is inductive and mesomeric.[23] In fact, the *meta*-position on the phenyl ring in BAn-(3)-F with respect to the fluorine atoms is the most electron-deficient, because it is affected only by the inductive electron-withdrawing character of the fluorine atom. Contrary to this, in the case of BAn-(2)-F, BAn-(4)-F, and BAn-(2,4)-F, the coordinating carbon of the phenyl ring is less electron-deficient, because the electron-withdrawing effect of the fluorine atom is compensated for by its electron-donating mesomeric character. The emission maximum for BAn-(3,4,5)-F in the solution state was observed at *ca.* 449 nm. From the spectra in Fig. 3b, one clearly observes a significant blue shift in the emission maximum for BAn-(3,5)-CF_3 (λ_{max} = 440 nm) relative to that for the F-substituted BAnFs, by 5–9 nm, due to the shortened π-conjugation of the distorted structure in the end-capping groups. When transferring from the solution to the solid state, the emission maxima of the BAnFs compounds show almost no red-shift, indicating the aggregation effect does not occur in the films of the synthesized compounds. It also indicates a very weak intermolecular interaction in the solid state, arising from the non-coplanar structure. The PL spectra of these BAnFs were also studied in different organic solvents. As shown in Fig. 4, the PL spectra of the BAnFs exhibit red-shifts of 37–42 nm when the solvent polarity is raised from 2.4 (toluene) to 5.8 (acetonitrile). This phenomenon is consistent with a variety of the excited states from the locally excited state (LE) to an excited state with the strong charge transfer (CT) character involving the TICT mechanism of the 9,9′-bianthracene core.[25] The full width at half maximum (FWHM) values in films of BAn-(2)-F, BAn-(3)-F, BAn-(4)-F, BAn-(2,4)-F, BAn-(3,4,5)-F and BAn-(3,5)-CF_3 were 53, 55, 52, 52, 48, and 48 nm, respectively.

We measured the fluorescence quantum yields (Φ_f) of the BAnFs in a dilute CH_2Cl_2 solution using quinine sulfate as a standard (Φ_f = 0.56 in 1.0 M H_2SO_4 solution) at room temperature. As shown in Table 1, the location of the fluorine substituents on the phenyl group seems to be of importance. The comparison of experimental values reveals an increase of Φ_f by insertion of F or CF_3 substituents, and the Φ_f increases with the number of F atoms. For example, the Φ_fs of BAn-(2)-F and BAn-(2,4)-F with mono- and di-F substituents were 0.55 and 0.69, respectively. BAn-(3,5)-CF_3, with the CF_3 substituents, had the highest quantum yield (0.99) in a CH_2Cl_2 solution, indicating that the CF_3 substituent plays a greater role in increasing

Table 1 Physical properties of the BAnFs

Compound	$\lambda_{max}^{Abs\ a,b}$ (nm)	$\lambda_{max}^{PL\ a,b}$ (nm)	$\Phi_f{}^c$	$T_g/T_m{}^d$ (°C)	$E_{ox}{}^e$ (V)	HOMO/LUMO^{exp} $(E_g^{opt})^f$ (eV)	HOMO/LUMO^{cal} $(\Delta E_{HOMO-LUMO})^g$ (eV)
BAn-(2)-F	259, 340, 358, 378, 400/270, 342, 361, 382, 404	449/448	0.55	168/299, 328	0.90	−5.70/−2.66 (3.04)	−5.26/−1.77 (3.49)
BAn-(3)-F	260, 340, 359, 379, 400/269, 343, 362, 383, 405	445/447	0.48	167/362	0.93	−5.73/−2.67 (3.06)	−5.29/−1.81 (3.48)
BAn-(4)-F	260, 340, 359, 379, 401/266, 343, 362, 383, 405	449/447	0.41	167/347	0.88	−5.68/−2.63 (3.05)	−5.25/−1.77 (3.48)
BAn-(2,4)-F	259, 338, 358, 378, 400/270, 342, 362, 382, 405	448/443	0.69	156/248, 322	0.97	−5.77/−2.69 (3.08)	−5.28/−1.82 (3.46)
BAn-(3,4,5)-F	259, 339, 358, 378, 400/264, 342, 360, 380, 403	449/445	0.93	NA/387	0.94	−5.74/−2.67 (3.07)	−5.47/−1.99 (3.48)
BAn-(3,5)-CF_3	259, 340, 358, 379, 400/257, 341, 359, 378, 400	440/438	0.99	NA/NA	1.06	−5.86/−2.78 (3.08)	−5.67/−2.18 (3.49)

[a] Measured in CH_2Cl_2. [b] Measured in solid thin film on quartz plates. [c] Determined in CH_2Cl_2 using quinine sulfate ($\Phi_{PL} = 0.56$ in 1.0 M H_2SO_4 solution) as standard. [d] T_g: glass-transition temperature; T_m: melting point; NA: not available. [e] Determined from the onset of oxidation potentials; measured in CH_3CN; all of the potentials are reported relative to ferrocene, which was used as the internal standard in each experiment. The ferrocene oxidation potential was located at 0.16 V, relative to the Pt-wire reference electrode. [f] The HOMO and LUMO energies were determined from cyclic voltammetry and the absorption onset. $E_{HOMO} = -(qE_{ox} + 4.8)$ eV; $E_{LUMO} = E_{HOMO} + E_g^{opt}$. [g] Values from DFT calculation.

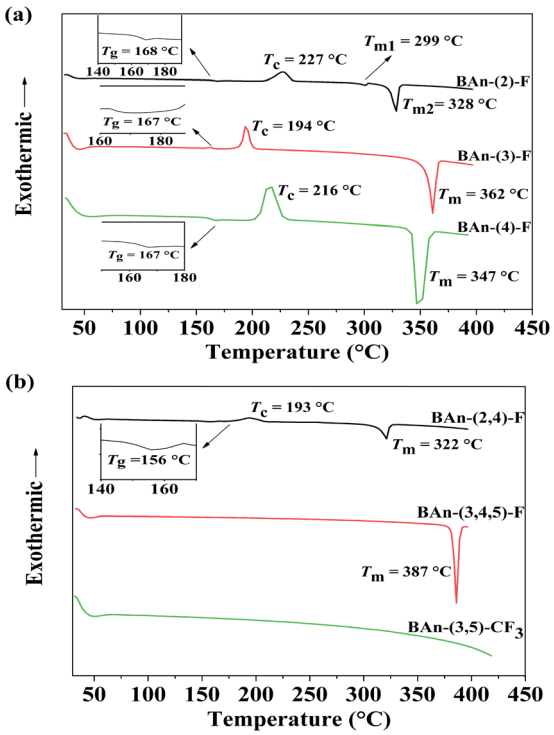

Fig. 2 DSC scans of the BAnFs recorded under nitrogen during the second heating cycle at a scan rate of 10 °C min^{-1}.

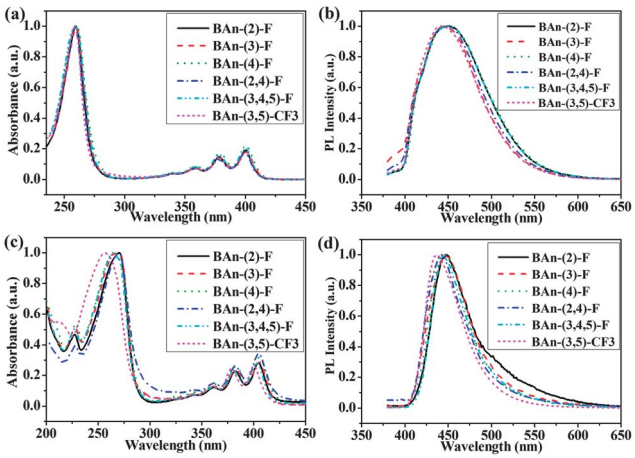

Fig. 3 (a) Absorption spectra of BAnFs in CH_2Cl_2. (b) PL spectra of BAnFs in CH_2Cl_2. (c) Absorption of BAnFs in films. (d) PL spectra of BAnFs in films.

the Φ_f. The extremely high quantum yield and narrow FWHM of BAn-(3,5)-CF_3 makes it an excellent candidate for use as an efficient blue-light-emitting material in OLEDs.

2.4 Electrochemical properties

Cyclic voltammetric (CV) studies were performed to calculate the HOMO and LUMO values for the BAnFs. The oxidation and reduction CV experiments were carried out in solutions of a 0.1 M supporting electrolyte ($[Bu_4N]ClO_4$) and 1 mM substrate in dry acetonitrile under an nitrogen atmosphere using ferrocene as an internal standard. The voltammograms for the BAnFs are shown in Fig. 5. All the compounds exhibit oxidation waves at potentials higher than that observed for ferrocene. The electrochemical properties, as well as the energy level parameters of the BAnFs, are listed in Table 1. From the first oxidation onset potential, all the HOMO energy levels of the BAnFs were estimated to be −5.68 to −5.86 eV. The LUMO energy levels of the BAnFs were calculated to be in the range −2.63 to −2.78 eV, from the absorption edge of the optical absorption spectra. BAn-(3)-F, with a mono-F substituent at the *meta*-position, has a slightly lower HOMO level (−5.73 eV) than that at the *ortho*-position (−5.70 eV) or *para*-position (−5.68 eV). The HOMO energy level decreases with the number of F atoms. By increasing the number of the highly electronegative F substituents on the phenyl groups, the electron-withdrawing capability of the F substituted phenyl groups is enhanced. For example,

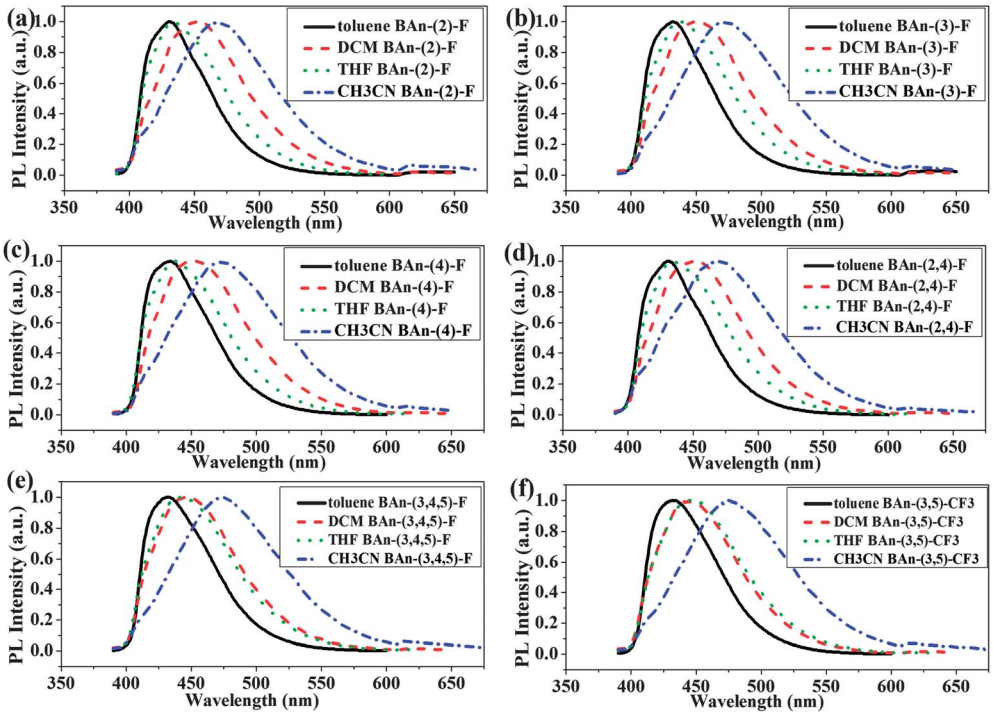

Fig. 4 PL spectra of the BAnFs in various solvents.

the HOMO levels of BAn-(2)-F and BAn-(2,4)-F with mono- and di-F substituents were −5.70 and −5.77 eV, respectively. A similar situation was observed by our group for 9,9′-spirobifluorene,[24] Chen *et al.* for perylene bisimides and Gade *et al.* for 2,9-bisaryl-tetraazaperopyrene.[26] The CF_3 substituent at the *meta*-position (BAn-(3,5)-CF_3) resulted in the lowest HOMO level (−5.86 eV) for the stronger electron-withdrawing capability of CF_3 substituent. As seen from Table 1, the experimental HOMOs and LUMOs are in excellent agreement with the calculated values. The BAnFs had wide optical energy gaps (E_g)

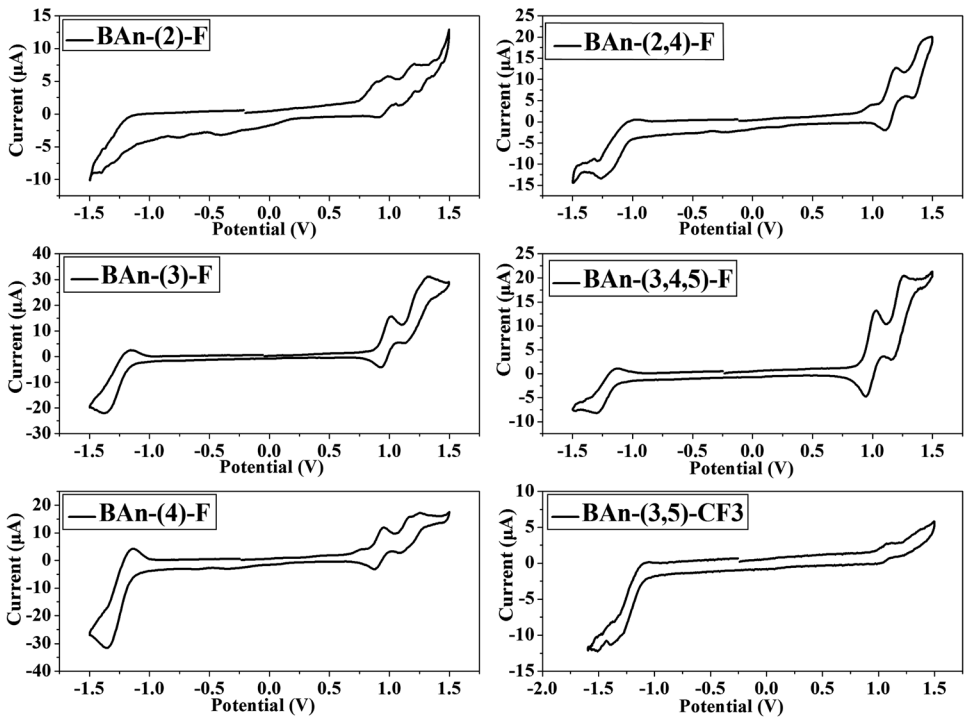

Fig. 5 Cyclic voltammograms of the BAnFs in CH_3CN.

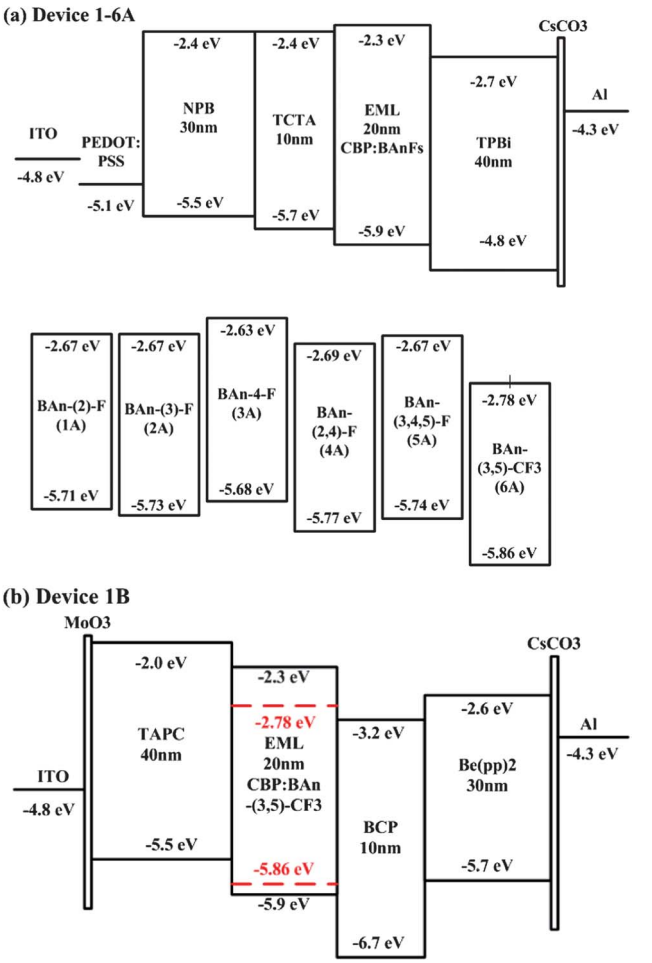

Fig. 6 (a) Structures of device 1-6A and energy levels of the BAnFs. (b) Structure of device 1B.

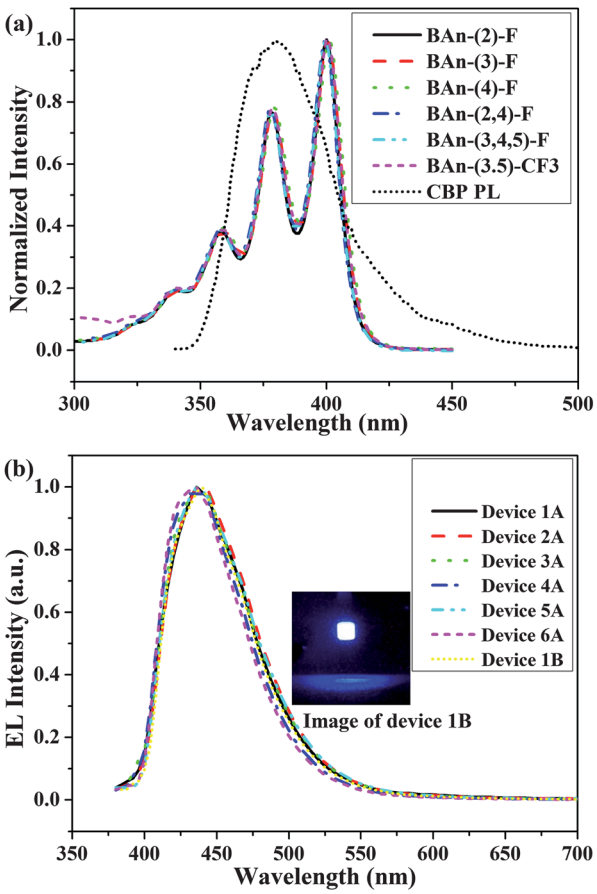

Fig. 7 (a) PL spectra of CBP and absorption spectra of BAnFs in CH_2Cl_2. (b) EL spectra of BAnF-doped devices at 8 V and emission photograph of device 1B.

of 3.04 to 3.08 eV. Accordingly, the BAnFs could be expected to be suitable candidates for deep blue emitters.

2.5 Electroluminescent properties

In order to achieve a deep-blue EL, we chose BAnFs as the dopants for device fabrication. In these devices, the well known ambipolar conductive 4,4′-bis(*N*-carbazolyl)biphenyl (CBP) was used as host material.[27] As shown in Fig. 6a, the BAnF-doped devices (1-6A) were fabricated with the following configuration: indium tin oxide (ITO)/poly(3,4-ethylenedioxythiophene) : poly(styrenesulfonate) (PEDOT : PSS) (30 nm)/4,4′-bis[*N*-(1-naphthyl)-*N*-phenyl-amino]biphenyl (NPB) (30 nm)/4,4′,4″-tris(carbazol-9-yl)-triphenylamine (TcTa) (10 nm)/blue emitting layer (EML) (20 nm)/1,3,5-tris(1-phenyl-1*H*-benzimidazol-2-yl)benzene (TPBi) (40 nm)/$CsCO_3$ (3 nm)/Al (100 nm). PEDOT : PSS was used as a hole injection layer (HIL), NPB was used as a hole transporting layer (HTL), TcTa was used as an exciton blocking layer, TPBi was used as an electron transporting layer (ETL) and exciton blocking layer, and $CsCO_3$ was used as an electron injection layer (EIL). Each dopant was co-evaporated with CBP to give the optimal doping concentration of 5 wt% in the EML (we fabricated several devices with various doping concentrations of 3, 5, 7, 9 wt%). Since the spectral overlap efficiency between the PL spectra of CBP and absorption spectra of the dopants is very high (Fig. 7a), Förster energy transfer was efficient from the CBP host to the dopants. Fig. 7b shows the normalized EL spectra for the BAnF-doped devices. All of the blue EL spectra of the BAnF-doped devices are very similar to the corresponding PL spectra in the thin-film state, which indicates that the EL emissions are mainly contributed by the fluorescence of the BAnFs. The CIE chromaticity coordinates of the BAnF-doped devices are in the range (0.154–0.156, 0.073–0.087) at 8 V, which show the extremely pure deep-blue emissions with peaks at 435–440 nm and meet the NTSC blue standard. The BAnFs-doped devices show narrow FWHMs of 63–69 nm without excimer or exciplex emission. Moreover, Fig. 8 shows the CIE values of all the devices in response to the driving voltage; a negligible EL color shift was observed when the driving voltage was increased from 4 to 10 V. It also suggests that the electron–hole pairs for recombination are well confined in the blue emitter region. Fig. 9 exhibits the current density–voltage–luminance–efficiency (J–V–L–η) characteristics of the BAnF-doped devices. The key device performance parameters and EL emission characteristics are summarized in Table 2. The BAnF-doped devices display low turn-on voltages (at a luminance of 1 cd m^{-2}) no greater than 4.5 V. The current efficiency and power efficiency of these devices are in the range 1.28–2.40

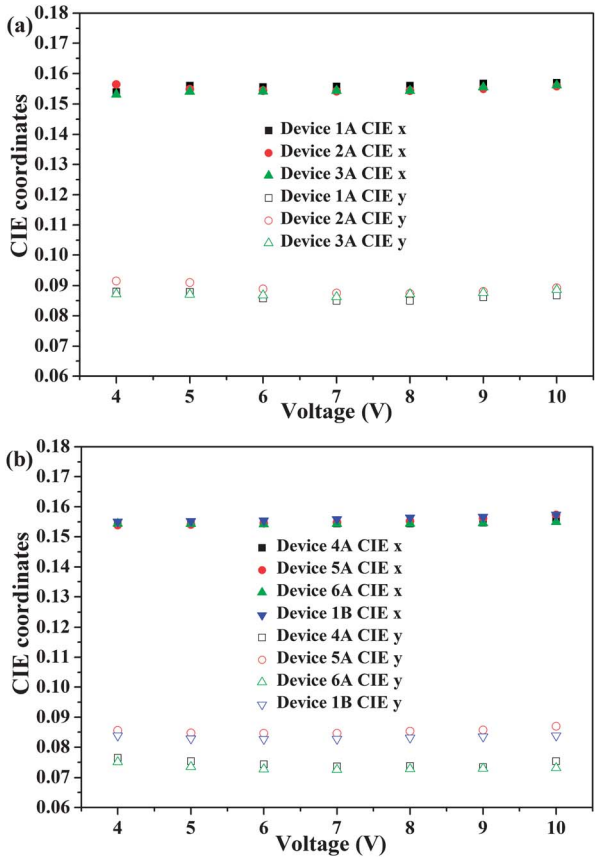

Fig. 8 CIE coordinates of EL spectra in response to the driving voltage of BAnF-doped devices from 4 V to 10 V.

cd A^{-1} and 0.87–1.96 lm W^{-1}, respectively. These EL behaviors are in excellent agreement with the Φ_fs. Notably, the device 6A with BAn-(3,5)-CF_3 as the dopant, achieves the best EL performance, with a maximum external quantum efficiency (EQE) as high as 4.65% (Fig. 10), a maximum current efficiency of 2.40 cd A^{-1}, a maximum power efficiency of 1.96 lm W^{-1} and a pure blue emission at CIE (0.154, 0.073). The excellent EL efficiency of the BAn-(3,5)-CF_3-doped device can be attributed mainly to its high Φ_f (0.99) and the efficient energy transfer from CBP to the BAn-(3,5)-CF_3 dopant to form LEs (the electron–hole pair localizes at one anthracene plane). What is more, the electron trapping followed by the direct recombination with the hole at the dopant sites could additionally contribute to the enhanced EL efficiency. Charge carriers direct recombination by trapping at the dopant sites will produce both LEs and perpendicular TICT-states (the electron and hole of a bound electron–hole pair may reside on two anthracene rings of one molecule respectively). Due to the lack of a significant coupling between the ground and excited state, a perpendicular TICT emission is forbidden. While the TICT-state is a spin-orbit, charge-transfer intersystem crossing mechanism, it is possible that the transition of $^1CT \leftrightarrow {}^3CT$ is allowed, due to the small energy splitting between them, especially in the perpendicular orientation between the donor and accepter.[28] The 9,9′-bianthracene-cored fluorescence emitters with particular TICT characteristics realize the electron–hole recombination *via* an intramolecular conversion from the TICT-state (precursor) to a radiative singlet exciton (final state), *e.g.*, $^1CT \rightarrow {}^1LE$ and $^3CT \rightarrow {}^1CT \rightarrow {}^1LE$.[18] For the BAn-(3,5)–$CF_3$–doped EL device, the singlet generation fraction is more than 25%. In addition, the LUMO level of

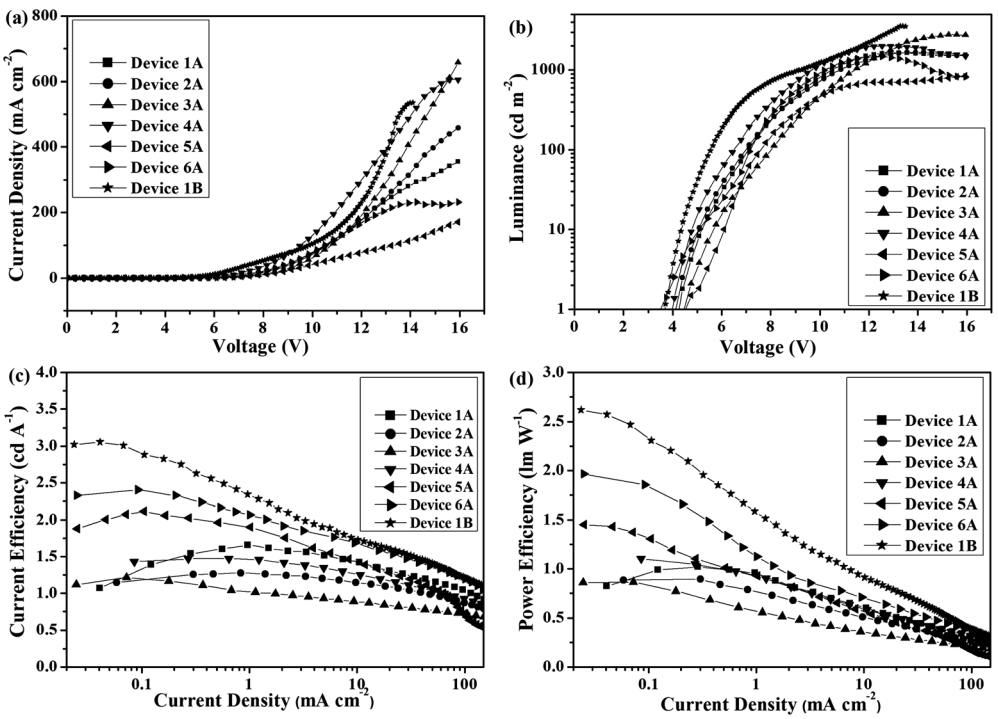

Fig. 9 (a) Current density–voltage curves. (b) Brightness–voltage curves. (c) Current efficiency–current density curves. (d) Power efficiency–current density curves for BAnFs-doped devices.

Table 2 EL performance of deep-blue devices with 5 wt% BAnFs doped in the EML

Device	EML	λ_{max}^{EL} (nm)	V_{on} [b] (V)	L_{max} [c] (cd m^{-2})	η_{ext} [d] (%)	η_c [d] (cd A^{-1})	η_p [d] (lm W^{-1})	FWHM (nm)	CIE (x, y)[a]
1A	CBP:BAn-(2)-F	438	4.2	1647	2.67	1.66	1.02	67	(0.156, 0.085)
2A	CBP:BAn-(3)-F	440	4.1	1669	1.99	1.28	0.89	69	(0.154, 0.087)
3A	CBP:BAn-(4)-F	437	4.4	2766	1.86	1.22	0.87	68	(0.154, 0.087)
4A	CBP:BAn-(2,4)-F	435	4.0	2016	2.75	1.47	1.10	65	(0.154, 0.074)
5A	CBP:BAn-(3,4,5)-F	437	4.5	838	3.42	2.11	1.45	67	(0.155, 0.085)
6A	CBP:BAn-(3,5)-CF_3	434	3.5	1471	4.65	2.40	1.96	63	(0.154, 0.073)
1B	CBP:BAn-(3,5)-CF_3	435	3.7	3588	5.02	3.05	2.62	66	(0.156, 0.083)

[a] Values collected at 8 V. [b] Turn-on voltage at 1 cd m^{-2}. [c] Maximum luminance. [d] Values collected at a peak efficiency.

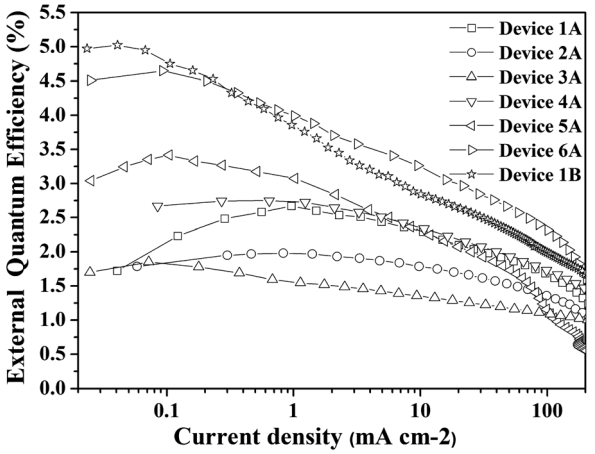

Fig. 10 External quantum efficiency (EQE) at different current densities for BAnFs-doped devices.

BAn-(3,5)-CF_3 (−2.78 eV) is the lowest of the BAnFs; a low-lying LUMO level implies a facilitated electron injection and an improved hole–electron balance, where an improved hole–electron balance in charge injection enhances the efficiency of the devices.

We believe that further improvements in the device performance can be achieved through an energy level adjustment between neighboring layers, charge mobility matching, and so on. So, we fabricated device 1B, as shown in Fig. 6b, the configuration of BAn-(3,5)-CF_3-doped device 1B is as below: ITO/molybdenum trioxide (MoO_3) (3 nm)/4,4′-cyclohexylidene-bis[*N*,*N*-bis(4-methylphenyl)aniline] (TAPC) (40 nm)/EML (20 nm)/2,9-dimethyl-4,7-diphenyl-1,10-phenanthroline (BCP) (10 nm)/bis[2-(2-hydroxyphenyl)-pyridine]beryllium ($Be(pp)_2$) (30 nm)/$CsCO_3$ (3 nm)/Al (100 nm), in which MoO_3 and $CsCO_3$ were the HIL and the EIL, respectively, TAPC was the HTL and the exciton blocking layer, $Be(pp)_2$ was the ETL, BCP was the exciton blocking layer, BAn-(3,5)-CF_3 was co-evaporated with CBP to give a 5 wt% dopant content in the EML. Due to the high electron mobility of $Be(pp)_2$, carrier transmission has been further balanced. Moreover, TAPC and BCP have a better exciton blocking ability to confine the excitons in the EML. Compared to a maximum current efficiency of 2.40 cd A^{-1}, a maximum power efficiency of 1.96 lm W^{-1}, and a maximum EQE of 4.65% for device 6A, the maximum current efficiency and the maximum power efficiency of device 1B are accordingly increased to 3.05 cd A^{-1} and 2.62 lm W^{-1}, corresponding to 5.02% of the maximum EQE. Additionally, a pure blue emission at CIE (0.156, 0.083) has been achieved with the emission peaking at *ca.* 435 nm. The performance of the BAn-(3,5)-CF_3-doped device was outstanding compared to previously reported results for deep-blue organic electroluminescent devices.[13,14]

3. Conclusions

In summary, a series of deep-blue materials of fluorinated 9,9′-bianthracene derivatives (BAnFs) have been successfully prepared by Suzuki coupling reactions, in high yields. We have demonstrated that the absorption, emission, electrochemical properties, and OLED performances are significantly affected by the introduction of electron-withdrawing substituents such as F and CF_3 into the 9,9′-bianthracene core, which were supported by theoretical calculations employing the B3LYP functional. The doped EL device with BAn-(3,5)-CF_3 as the dopant achieved an maximum external quantum efficiency (EQE) of 5.02% (3.05 cd A^{-1}) in the deep-blue visible region with excellent CIE chromaticity coordinates (0.156, 0.083) that meet the NTSC standard blue coordinates. The BAn-(3,5)-CF_3-doped device exhibits a high EQE, which shows a potential application as an emitter for pure blue devices.

4. Experimental

4.1 General information

The manipulation involving air-sensitive reagents was performed under an inert atmosphere of dry nitrogen. Commercially available reagents were used without further purification unless otherwise stated. 9,10-Anthracenedione, 2-fluorophenylboronic acid, 3-fluorophenylboronic acid, 4-fluorophenylboronic acid, 2,4-difluorophenylboronic acid, 3,4,5-trifluorophenylboronic acid, 3,5-bis(trifluoromethyl)phenylboronic acid, and tetrakis(triphenylphosphine)palladium were purchased and used as received. The photoluminescence (PL) and absorption spectra were recorded on a Horiba Jobin Yvon Fluoromax-4 spectrophotometer and a Hitachi UV 3010 spectrophotometer, respectively. To measure the fluorescence quantum yields (Φ_f), degassed solutions of the compounds in CH_2Cl_2 were prepared. The concentration was adjusted so that the absorbance of the solution would be lower than 0.1. The

excitation was performed at 340 nm, and quinine sulfate in 1.0 M H_2SO_4 solution, which has a $\Phi_f = 0.56$, was used as a standard. The difference between the refractive index of the solvent and that of the standard should also be counted. The glass transition temperatures (T_g) were determined with a differential scanning calorimeter (DSC, TA instruments DSC200PC) at a heating rate of 10 °C min^{-1} under a nitrogen atmosphere. Cyclic voltammetry (CV) was performed using a Princeton Applied Research model 273 A potentiostat at a scan rate of 100 mV s^{-1}. All the experiments were carried out in a three electrode compartment cell with a Pt-sheet counter electrode, a glassy carbon working electrode and a Pt-wire reference electrode. The supporting electrolyte used was a 0.1 M tetrabutylammonium perchlorate ($[Bu_4N]ClO_4$) solution in dry acetonitrile. The cell containing the solution of the sample (1 mM) and the supporting electrolyte was purged with nitrogen gas thoroughly before scanning for its oxidation and reduction properties. Ferrocene was used for the potential calibration in each measurement. All the potentials were reported relative to the ferrocene-ferrocenium (Fc/Fc^+) couple, whose oxidation potential was +0.16 V relative to the reference electrode. The oxidation and reduction potentials were determined by taking the average of the anodic and cathodic peak potentials. The HOMO and LUMO values were estimated by using the following general equation: $E_{HOMO} = -(qE_{ox} + 4.8)$ eV; $E_{LUMO} = E_{HOMO} - E_g^{opt}$, which were calculated using the internal standard ferrocene value of −4.8 eV with respect to the vacuum level.

4.2 Preparation of blue emitters BAnFs

9,9′-Bianthracene and 10,10′-dibromo-9,9′-bianthracene were synthesized according to the literature.[29] A series of novel fluorinated 9,9′-bianthracene derivatives were synthesized by the Suzuki coupling reaction between brominated 9,9′-bianthracene and the respective fluorinated phenylboronic in the presence of a palladium catalyst, with yields ranging from 83 to 96% (Scheme 1). THF (30 mL) and an aqueous solution of K_2CO_3 (2.0 M, 10 mL) were added to a flask containing 10,10′-dibromo-9,9′-bianthracene (2.34 mmol), the fluorinated phenylboronic (8 mmol) and $Pd(PPh_3)_4$ (0.35 mmol) under nitrogen. The reaction mixture was heated to reflux and maintained at this temperature for 24 h. When the reaction was completed (judging from thin-layer chromatography), water was added to quench the reaction. Then, the products were extracted with CH_2Cl_2. The organic portion was washed with brine, dried over anhydrous $MgSO_4$, and concentrated by evaporating off the solvent. The solid was absorbed on silica gel and purified by column chromatography using light petrol ether–ethyl acetate as the eluent to give the product.

10,10′-Bis(2-fluorophenyl)-9,9′-bianthracene (BAn-(2)-F). 1.13 g, pale yellow solid, yield: 89%. T_m = 328 °C. ^{1}H NMR ($CDCl_3$, 400 MHz): δ 7.18–7.26 (m, 10H), 7.27–7.30 (m, 4H), 7.37–7.51 (m, 4H), 7.60–7.68 (m, 4H), 7.78–7.82 (d, J = 8.8 Hz, 4H). Anal. calcd for $C_{40}H_{24}F_2$: C, 88.54; H, 4.46. Found: C, 88.60; H, 4.35%.

10,10′-Bis(3-fluorophenyl)-9,9′-bianthracene (BAn-(3)-F). 1.18 g, pale yellow solid, yield: 93%. T_m = 362 °C. ^{1}H NMR ($CDCl_3$, 400 MHz): δ 7.17–7.25 (m, 10H), 7.29–7.32 (d, J = 8.4 Hz, 2H), 7.33–7.39 (t, 4H), 7.41–7.43 (d, J = 7.6 Hz, 2H), 7.61–7.68 (q, 4H), 7.78–7.81 (d, J = 8.8 Hz, 4H). Anal. calcd for $C_{40}H_{24}F_2$: C, 88.54; H, 4.46. Found: C, 88.48; H, 4.38%.

10,10′-Bis(4-fluorophenyl)-9,9′-bianthracene (BAn-(4)-F). 1.15 g, white solid, yield: 91%. T_m = 347 °C. ^{1}H NMR ($CDCl_3$, 400 MHz): δ 7.16–7.19 (m, 4H), 7.22–7.26 (t, 4H), 7.33–7.40 (q, 8H), 7.57–7.62 (q, 4H), 7.77–7.81 (d, J = 8.8 Hz, 4H). Anal. calcd for $C_{40}H_{24}F_2$: C, 88.54; H, 4.46. Found: C, 88.50; H, 4.55%.

10,10′-Bis(2,4-bifluorophenyl)-9,9′-bianthracene (BAn-(2,4)-F). 1.22 g, pale yellow solid, yield: 90%. T_m = 322 °C. ^{1}H NMR ($CDCl_3$, 400 MHz): δ 7.17–7.23 (m, 12H), 7.38–7.41 (m, 4H), 7.53–7.61 (q, 4H), 7.74–7.61 (d, J = 8.0 Hz, 4H). Anal. calcd for $C_{40}H_{22}F_4$: C, 83.03; H, 3.83. Found: C, 83.13; H, 3.75%.

10,10′-Bis(3,4,5-trifluorophenyl)-9,9′-bianthracene (BAn-(3,4,5)-F). 1.38 g, white solid, yield: 96%. T_m = 387 °C. ^{1}H NMR ($CDCl_3$, 400 MHz): δ 7.18–7.20 (m, 8H), 7.27–7.31 (t, 4H), 7.38–7.43 (m, 4H), 7.73–7.78 (d, J = 8.8 Hz, 4H). Anal. calcd for $C_{40}H_{20}F_6$: C, 78.17; H, 3.28. Found: C, 78.20; H, 3.17%.

10,10′-Bis(3,5-bis(trifluoromethyl)phenyl)-9,9′-bianthracene (BAn-(3,5)-CF_3). 1.39 g, white solid, yield: 83%. ^{1}H NMR ($CDCl_3$, 400 MHz): δ 7.22–7.24 (d, J = 6.4 Hz, 8H), 7.42–7.45 (m, 4H), 7.62–7.64 (d, J = 8.8 Hz, 4H), 8.14–8.16 (d, J = 6.8 Hz, 4H). Anal. calcd for $C_{44}H_{22}F_{12}$: C, 67.87; H, 2.85. Found: C, 67.75; H, 2.91%.

4.3 Device fabrication and testing

The OLEDs were fabricated by thermal evaporation onto a cleaned glass substrate, pre-coated with transparent and conductive indium tin oxide (ITO). Prior to the organic layer deposition, the ITO substrates were exposed to a UV-ozone flux for 10 min, following degreasing in acetone and isopropyl alcohol (IPA). All of the organic materials were purified by temperature-gradient sublimation in a vacuum. The devices were fabricated by the conventional vacuum deposition of the organic layers, $CsCO_3$ and an Al cathode onto an ITO-coated glass substrate under a base pressure lower than 1×10^{-3} Pa. The thickness of each layer was determined by a quartz thickness monitor. The voltage–current density (V–J) and voltage–brightness (V–L) as well as the current density–current efficiency (J–η_c) and current density–power efficiency (J–η_p) curve characteristics of the devices were measured with a Keithley 2602 and Source Meter. All the measurements were carried out at room temperature under ambient conditions.

Acknowledgements

This work was financially supported by the Basic Research Program of China (2013CB328705), the National Natural Science Foundation of China (Grant nos 61275034, 61106123 and 61308093), the Fundamental Research Funds for the Central Universities (Grant no. xjj2012087) and the China Postdoctoral Science Foundation (Grant no. 20110491653). The supporting information is available online from the author.

References

1 C. W. Tang and S. A. Van Slyke, *Appl. Phys. Lett.*, 1987, **51**, 913.

2 L. S. Hung and C. H. Chen, *Mater. Sci. Eng., R*, 2002, **39**, 143.

3 S. R. Forrest, *Nature*, 2004, **428**, 911.

4 Y. Sun, N. C. Giebink, H. Kanno, B. Ma, M. E. Thompson and S. R. Forrest, *Nature*, 2006, **440**, 908.

5 (*a*) M. T. Lee, H. H. Chen, C. H. Liao, C. H. Tsai and C. H. Chen, *Appl. Phys. Lett.*, 2004, **85**, 3301; (*b*) M. T. Lee, C. H. Liao, C. H. Tsai and C. H. Chen, *Adv. Mater.*, 2005, **17**, 2493.

6 C. W. Tang, S. A. VanSlyke and C. H. Chen, *J. Appl. Phys.*, 1989, **65**, 3610.

7 (*a*) Y. H. Kim, D. C. Shin, S. H. Kim, C. H. Ko, H. S. Yu, Y. S. Chae and S. K. Kwon, *Adv. Mater.*, 2001, **13**, 1690; (*b*) J. Shi and C. W. Tang, *Appl. Phys. Lett.*, 2002, **80**, 3201; (*c*) Y. Kan, L. Wang, L. Duan, Y. Hu, G. Wu and Y. Qiu, *Appl. Phys. Lett.*, 2004, **84**, 1513; (*d*) Y. H. Kim, H. C. Jeong, S. H. Kim, K. Y. Yang and S. K. Kwon, *Adv. Funct. Mater.*, 2005, **15**, 1799; (*e*) P.-I. Shih, C.-Y. Chuang, C.-H. Chien, E. W.-G. Diau and C.-F. Shu, *Adv. Funct. Mater.*, 2007, **17**, 3141; (*f*) Y. Y. Lyu, J. Kwak, O. Kwon, S. H. Lee, D. Kim, C. Lee and K. Char, *Adv. Mater.*, 2008, **20**, 2720; (*g*) C. H. Chien, C. K. Chen, F. M. Hsu, C. F. Shu, P. T. Chou and C. H. Lai, *Adv. Funct. Mater.*, 2009, **19**, 560; (*h*) C. J. Zheng, W. M. Zhao, Z. Q. Wang, D. Huang, J. Ye, X. M. Ou, X. H. Zhang, C. S. Lee and S. T. Lee, *J. Mater. Chem.*, 2010, **20**, 1560; (*i*) K. H. Lee, J. K. Park, J. H. Seo, S. W. Park, Y. S. Kim, Y. K. Kim and S. S. Yoon, *J. Mater. Chem.*, 2011, **21**, 13640; (*j*) S. H. Lin, F. I. Wu, H. Y. Tsai, P. Y. Chou, H. H. Chou, C. H. Cheng and R. S. Liu, *J. Mater. Chem.*, 2011, **21**, 8122; (*k*) H. Park, J. Lee, I. Kang, H. Y. Chu, J. I. Lee, S. K. Kwon and Y. H. Kim, *J. Mater. Chem.*, 2012, **22**, 2695.

8 (*a*) C. C. Wu, Y. T. Lin, K. T. Wong, R. T. Chen and Y. Y. Chien, *Adv. Mater.*, 2004, **16**, 61; (*b*) Z. P. Silu, X. Zhang, J. Tang, C. S. Lee and S.-T. Lee, *J. Phys. Chem. C*, 2008, **112**, 2165.

9 (*a*) S. E. Shaheen, G. E. Jabbour, M. M. Morrell, Y. Kawabe, B. Kippelen, N. Peyghambarian, M.-F. Nabor, R. Schlaf, E. A. Mash and N. R. Armstrong, *J. Appl. Phys.*, 1998, **84**, 2324; (*b*) F. I. Wu, P. I. Shih, M. C. Yuan, C. F. Shu, Z. M. Chung and E. W. G. Diau, *J. Mater. Chem.*, 2005, **15**, 4753; (*c*) Y. Duan, Y. Zhao, P. Chen, J. Li, S. Liu, F. He and Y. Ma, *Appl. Phys. Lett.*, 2006, **88**, 263503.

10 (*a*) S. Tao, Z. Peng, X. Zhang, P. Wang, C. S. Lee and S. T. Lee, *Adv. Funct. Mater.*, 2005, **15**, 1716; (*b*) C. Tang, F. Liu, Y. J. Xia, L. H. Xie, A. Wei, S. B. Li, Q. L. Fan and W. J. Huang, *J. Mater. Chem.*, 2006, **16**, 4074; (*c*) K. C. Wu, P. J. Ku, C. S. Lin, H. T. Shih, F. I. Wu, M. J. Huang, J. J. Lin, I. C. Chen and C. H. Cheng, *Adv. Funct. Mater.*, 2008, **18**, 67.

11 (*a*) A. P. Kulkami, A. P. Gifford, C. J. Tozola and S. A. Jenekhe, *Appl. Phys. Lett.*, 2005, **86**, 061106; (*b*) C. J. Tonzola, A. P. Kukarni, A. P. Gifford, W. Kaminsky and S. A. Jenekhe, *Adv. Funct. Mater.*, 2007, **17**, 863; (*c*) S. J. Lee, J. S. Park, K. J. Yoon, Y. I. Kim, S. H. Jin, S. K. Kang, Y. S. Gal, S. Kang, J. Y. Lww, J. W. Kang, S. H. Lww and H. D. Park, *Adv. Funct. Mater.*, 2008, **18**, 3922.

12 (*a*) H. T. Shih, C. H. Lin, H. S. Shih and H. C. Cheng, *Adv. Mater.*, 2002, **14**, 1409; (*b*) H. P. Rathnayake, A. Cirpan, P. M. Lahti and F. E. Karasz, *Chem. Mater.*, 2006, **18**, 560; (*c*) H. P. Rathnayake, A. Cirpan, Z. Delen, P. M. Lahti and F. E. Karasz, *Adv. Funct. Mater.*, 2007, **17**, 115.

13 (*a*) S. K. Kim, B. Yang, Y. Ma, J. H. Lee and J. W. Park, *J. Mater. Chem.*, 2008, **18**, 3376; (*b*) C. H. Wu, C. H. Chien, F. M. Hsu, P. I. Shih and C. F. Shu, *J. Mater. Chem.*, 2009, **19**, 1464; (*c*) C. J. Zheng, W. M. Zhao, Z. Q. Wang, D. Huang, J. Ye, X. M. Ou, X. H. Zhang, C. S. Lee and S. T. Lee, *J. Mater. Chem.*, 2010, **20**, 1560; (*d*) C. G. Zhen, Y. F. Dai, W. J. Zeng, Z. Ma, Z. K. Chen and J. Kieffer, *Adv. Funct. Mater.*, 2011, **21**, 699; (*e*) T. Peng, G. Li, Y. Liu, Y. Wu, K. Ye, D. Yao, Y. Yuan, Z. Hou and Y. Wang, *Org. Electron.*, 2011, **12**, 1068; (*f*) S. L. Lai, Q. X. Tong, M. Y. Chan, T. W. Ng, M. F. Lo, S. T. Lee and C. S. Lee, *J. Mater. Chem.*, 2011, **21**, 1206; (*g*) C. J. Kuo, T. Y. Li, C. C. Lien, C. H. Liu, F. I. Wu and M. J. Huang, *J. Mater. Chem.*, 2009, **19**, 1865.

14 (*a*) B. Ding, W. Zhu, X. Jiang and Z. Zhang, *Curr. Appl. Phys.*, 2008, **8**, 573; (*b*) K. H. Lee, J. N. You, S. Kang, J. Y. Lee, H. J. Kwon, Y. K. Kim and S. S. Yoon, *Thin Solid Films*, 2010, **518**, 6253; (*c*) S.-H. Lin, F.-I. Wu, H.-Y. Tsai, P.-Y. Chou, H.-H. Chou, C.-H. Cheng and R.-S. Liu, *J. Mater. Chem.*, 2011, **21**, 8122.

15 M. sarkar and A. Saman, *Acta Crystallogr., Sect. E: Struct. Rep. Online*, 2003, **59**, o1764.

16 (*a*) F. Schneider, E. Lippert and B. Bunsen-Ges, *Phys. Chem.*, 1968, **72**, 1155; (*b*) F. Schneider, E. Lippert and B. Bunsen-Ges, *Phys. Chem.*, 1970, **74**, 624; (*c*) M. Jurczok, T. Custavsson, J.-C. Mialocq and W. Rettig, *Chem. Phys. Lett.*, 2001, **344**, 357; (*d*) M. Jurczok, P. Plaza, M. M. Martin, Y. H. Meyer and W. Rettig, *Chem. Phys.*, 2000, **253**, 339; (*e*) N. Asami, T. Takaya, S. Yabumoto, S. Shigeto, H. Hamaguchi and K. Iwata, *J. Phys. Chem. A*, 2010, **114**, 6351; (*f*) X. Li, M. Liang, A. Chakraborty, M. Kondo and M. Maroncelli, *J. Phys. Chem. B*, 2011, **115**, 6592.

17 (*a*) K. Elich, S. Lebus, R. Wortmann, F. Petzke, N. Detzer and W. Liptay, *J. Phys. Chem.*, 1993, **97**, 9947; (*b*) A. Subaric-leitis, C. Monte, A. Roggan, W. Rettig, P. Zimmermann and J. Heinze, *J. Chem. Phys.*, 1990, **93**, 4543; (*c*) F. C. Grozema, M. Swart, R. W. J. Zijlstra, J. J. Piet, L. D. A. Siebbeles and P. Th. van Duijnen, *J. Am. Chem. Soc.*, 2005, **127**, 11019.

18 P. Zhang, W. Dou, Z. Ju, L. Yang, X. Tang, W. Liu and Y. Wu, *Org. Electron.*, 2013, **14**, 915.

19 J. Cornil, N. E. Gruhn, D. A. Dos Santos, M. Malagoli, P. A. Lee, S. Barlow, S. Thayumanavan, S. R. Marder, N. R. Armstrong and J. L. Brédas, *J. Phys. Chem. A*, 2001, **105**, 5206.

20 Z. Li, Z. Wu, B. Jiao, P. Liu, D. Wang and X. Hou, *Chem. Phys. Lett.*, 2012, **527**, 36.

21 J. S. Reddy, T. Kale, G. Balaji, A. Chandrasekaran and S. Thayumanavan, *J. Phys. Chem. Lett.*, 2011, **2**, 648.

22 M. L. Tang and Z. Bao, *Chem. Mater.*, 2011, **23**, 446.

23 F. Babudri, G. M. Farinola, F. Naso and R. Ragni, *Chem. Commun.*, 2007, 1003.
24 (*a*) Z. Li, Z. Wu, W. Fu, P. Liu, B. Jiao, D. Wang, G. Zhou and X. Hou, *J. Phys. Chem. C*, 2012, **116**, 20504; (*b*) Z. Li, B. Jiao, Z. Wu, P. Liu, L. Ma, X. Lei, D. Wang, G. Zhou, H. Hu and X. Hou, *J. Mater. Chem. C*, 2013, **1**, 2183.
25 (*a*) M. A. Kahlow, T. J. Kang and P. F. Barbara, *J. Phys. Chem.*, 1987, **91**, 6452; (*b*) J. Catalan, C. Diaz, V. Lopez, P. Perez and R. M. Claramunt, *J. Phys. Chem.*, 1996, **100**, 18392.
26 (*a*) H. Z. Chen, M. M. Ling, X. Mo, M. M. Shi, M. Wang and Z. Bao, *Chem. Mater.*, 2007, **19**, 816; (*b*) S. C. Martens, T. Riehm, S. Geib, H. Wadepohl and L. H. Gade, *J. Org. Chem.*, 2011, **76**, 609.
27 (*a*) C. Adachi, M. E. Thompson and S. R. Forrest, *IEEE J. Sel. Top. Quantum Electron.*, 2002, **8**, 372; (*b*) M. A. Baldo and S. R. Forrest, *Phys. Rev. B: Condens. Matter Mater. Phys.*, 2000, **62**, 10958.
28 H. V. Willigen, G. Jones and M. S. Farahat, *J. Phys. Chem.*, 1996, **100**, 3312.
29 (*a*) F. Bell and D. H. Waring, *J. Chem. Soc.*, 1949, 267; (*b*) U. Müller and M. Baumgarten, *J. Am. Chem. Soc.*, 1995, **117**, 5840.